GEOPHYSICAL RESEARCH LETTERS, VOL. 26, NO. 16, PAGES 2633-2636, AUGUST 15, 1999

Poleward-displaced electron precipitation from lightning-generated oblique whistlers

D. S. Lauben, U. S. Inan, T. F. Bell

Space, Telecommunications and Radioscience Laboratory, Stanford University

Abstract. New simulation results show that obliquely-propagating lightning-generated whistlers which fill vast volumes of the magnetosphere readily induce significant energetic electron precipitation over large regions of the ionosphere, depositing appreciable energy flux to the upper atmosphere at locations substantially poleward of the lightning source. These results provide a new interpretation for the observed spatial relationships between lightning discharges and subsequently disturbed ionospheric regions inferred from subionospheric signal perturbations (i.e. Trimpi events) reported in several lightning-induced electron precipitation (LEP) studies.

1. Introduction

The connection between lightning-induced electron precipitation (LEP) and transient perturbations to the upper atmosphere sufficient to perturb subionospheric VLF signals (i.e Trimpi events) has been recognized for some time in association with ducted whistlers which propagate between hemispheres parallel to the earth's magnetic field lines within field-aligned tubes of enhanced ionization [*Inan and Carpenter*, 1986]. Here we generalize to lightning-generated whistlers which propagate throughout vast volumes of the magnetosphere at *oblique* angles with respect to the magnetic field in the *absence* of ionization ducts, thereby inducing precipitation over correspondingly extensive ionospheric regions.

2. Oblique Whistler Precipitation

A new formulation by *Lauben* [1998] extends that of *Chang and Inan* [1985] for electron precipitation from ducted whistlers, employing the oblique-wave scattering equations of *Ristic-Djurovic et al.* [1998] to calculate the precipitation induced by discrete, lightning-generated oblique whistlers over a wide range of L-shells.

In Fig. 1a, impulsive broadband VLF (1-10 kHz) wave energy radiated by an individual lightning discharge (modeled as a vertically oriented dipole) located at geomagnetic latitude λ_s illuminates the base of the ionosphere over a broad range of latitudes and longitudes, with nominal subionospheric attenuation matching multi-mode waveguide models [*Poulsen et al.*, 1993]. A fraction of this wave energy couples through the horizontally-stratified ionosphere (at assumed vertical incidence), suffering additional latitude- and frequency-dependent attenuation from collisional losses therein [*Helliwell*, 1965], to excite a whistler-mode wave packet throughout a correspondingly broad region of the magnetosphere. Within the magnetosphere the wave energy follows refracting ray paths dictated by Snell's law applied to the collisionless, inhomogeneous, anisotropic, magnetized cold plasma, assumed to be in a state of diffusive equilibrium along the static, inhomogeneous dipole magnetic field lines $\mathbf{B_o}$ [*Inan and Bell*, 1977]. The ray and wave normal directions are generally at oblique angles with respect to $\mathbf{B_o}$ as shown (Fig. 1a) by, respectively, the bundle of ray paths (f=5 kHz shown) and series of short line segments rooted along L=2.6 (representative), the later which are also plotted vs. λ in Fig. 1b (lower panel). Further attenuation occurs as the wave energy spreads due to ray bundle defocusing and frequency-time (f-t) dispersion, the later arising from the variation in group velocity with f as depicted at time $t\sim 1/2$ s by the colored broadband wave packet (Fig. 1a) for which the low frequencies (1 kHz, blue) generally lag the high frequencies (10 kHz, red). These two factors together give typically >30 dB attenuation near $\lambda\sim 0$ relative to the ray injection points, as shown for L=2.6 also in Fig. 1b (upper panel). Multiplying by the incident lightning-ionosphere illumination profile at all ray injection points then yeilds an overall magnetospheric whistler spatial intensity pattern (next section) matching satellite overflight measurements of ground-based VLF transmitter signals [*Rastani et al.*, 1985].

The complete oblique-whistler model is calibrated in an absolute sense against *in-situ* measured oblique whistler wave normal angles and intensities (over f) at a point near the magnetic equator for a lightning source taken to be optimally located beneath the most direct ray paths. Fig. 2 shows dynamic wave normal angle and intensity spectrograms for just such an oblique whistler observed at L=2.7, λ=−1.3° by the POLAR satellite Plasma Wave Instrument [*Gurnett et al.*, 1995]. Here the wave normal angles are ∼120° (Fig. 2b), or equivalently, ∼60° from the local $-\mathbf{B_o}$ direction, confirming raytracing results (c.f. Fig. 1b, lower panel), while the intensities of the wave magnetic field components transverse to $\mathbf{B_o}$ range 10 to 30 pT (Fig. 2d), strong but not uncommon values for whistlers observed along the magnetic equator. The model lightning source strength is scaled to give these measured intensities at this point, which thus sets intensities for all points throughout the magnetosphere. Afterwards the lighting latitude λ_s is relocated at will (with strength held constant) to study the variation in whistler spatial intensity pattern and precipitation flux levels with lightning location.

Returning to Fig. 1a, with the whistler wave packet properties for a given lightning source specified throughout the magnetosphere, along each of a set of L-shells covering $1.6 \leq L \leq 4.2$, a series of northward-streaming energetic electron test-particle ensembles having velocity space distribution $f_v \sim 1/v^6$ (fitting typical E^{-3} energy dependence and scaled

Paper number 1999GL900374.
0094-8276/99/1999GL900374$05.00

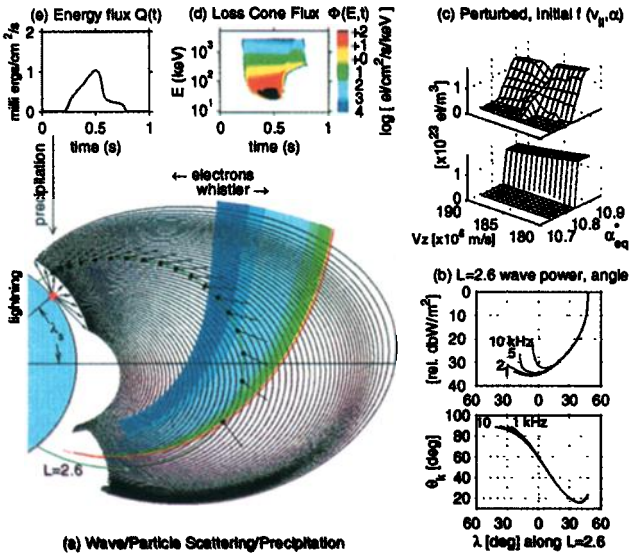

Figure 1. Oblique-whistler precipitation model. Counterclockwise from lower-left: (a) Lightning discharge at latitude λ_s illuminating the ionosphere, oblique whistler ray paths traced in the magnetic meridian, wave normal vectors along L=2.6, and broadband (blue=1 kHz to red=10 kHz) wave packet at time $t\sim 1/2$ s, (b) Simulated whistler magnetospheric attenuation and wave normal angle θ_k, (c) Initial and (representative) perturbed electron velocity space distributions, (d) Electron loss-cone flux $\Phi(E,t)$, and (e) Precipitation energy flux $Q(t)$ deposited to the upper atmosphere at L=2.6.

to give equatorial reference flux $j_o = 1 \times 10^8$ el/cm^2/s/keV at E_o=1 keV, after *Ristic-Djurovic et al.* [1998]) and having idealized void atmospheric loss cone (Fig. 1c, lower mesh) are injected into the southward-advancing wave packet at a succession of wavefront encounter latitudes (after *Chang and Inan* [1985]). The simulation tracks the frequency, wave normal angle and intensity seen by each test particle along its nominally adiabatic trajectory, calculating the particle scattering at those locations for which the condition for first-order gyroresonance is satisfied ($v_\parallel = (\omega_h - \omega)/k_\parallel$, see e.g. *Ristic-Djurovic et al.* [1998]), to find the fraction of particles from each ensemble deflected into the loss cone (Fig. 1d, upper mesh).

Since for the conditions considered herein particles are scattered predominantly via momentum deflection induced by the wave magnetic field (as opposed to acceleration by the wave electric field), and since in addition no appreciable particle Larmor-phase bunching occurs (as would indicate re-radiated coherent waves), no significant wave/particle energy exchange takes place and to first order, the waves are neither amplified nor damped during the interaction. This decoupling allows the whistler intensities to be established a-priori and applied (as done here) without subsequent adjustment.

Then under the simplifying assumption that all electrons entering the loss cone are immediately precipitated at their first encounter with the upper atmosphere in the northern hemisphere (Fig. 1a), the resulting electron precipitation flux energy-time signatures $\Phi(E,t)$ (integrated over the loss cone) and deposited integral energy flux $Q(t) = \int E\,\Phi\,dE$ are found, shown for L=2.6 in Figs. 1d and 1e, respectively. At other L-shells the precipitation signatures are similar, albeit with energy range, timing and flux levels differing in accord with the variation in resonance conditions, kinematics and available energetic electron flux along other field lines.

Subsequent to the first traverse of the oblique whistler through the magnetosphere, depending on the prevailing hot plasma density distribution the wave packet may in some cases undergo repeated magnetospheric reflections, propagating back and forth between conjugate locations, causing further precipitation [*Ristic-Djurovic et al.*, 1998], or, in other cases be completely Landau damped at the first reflection. For brevity we limit consideration herein to the primary precipitation pulse induced during the first traverse of the whistler.

3. Model Results

Fig. 3 shows the precipitation energy flux pulses $Q(t)$ deposited at the foot of L=2, 3 and 4 (upper panels) for the magnetospheric whistler spatial intensity patterns (lower panels) corresponding to lightning source magnetic latitudes λ_s=30°, 40° and 50° (each column, left to right, respectively). The straightforward kinematics governing propagation of the wave packet and travel-time of the scattered electrons from interaction to precipitation regions combine to give precipitation pulse onset, peak and termination times characteristic for each L-shell. Thus the earlier arrival at e.g. L=2 is due to both the shorter wave propagation paths and faster velocities of the generally higher resonant energy electrons for lower L-shells. Conversely, the later arrival (and sustained duration) at e.g. L=4 is due to the longer wave paths and slower velocities of the generally lower resonant energy electrons for higher L-shells. These *pulse timing* relationships are independent of lightning latitude since for any interaction region, the wave propagation time and res-

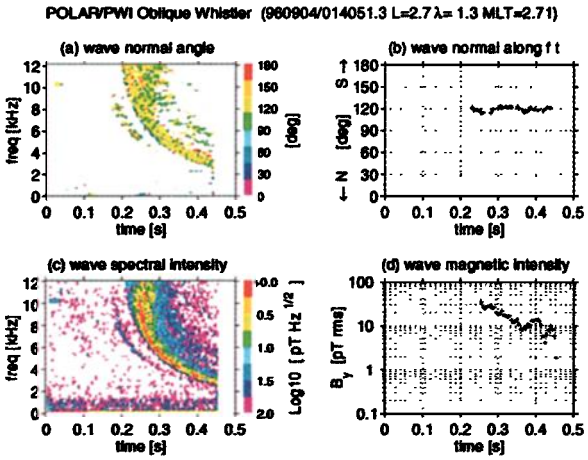

Figure 2. Measured oblique whistler. L=2.7. (a) Wave normal angle with respect to the static magnetic field $\mathbf{B_o}$ displayed in dynamic f-t format, (b) Wave normal angle along the whistler f-t trace, (c) Wave transverse (to $\mathbf{B_o}$) magnetic field dynamic spectral intensity, (d) Wave magnetic field intensity in a 140 Hz bandwidth along the whistler f-t trace.

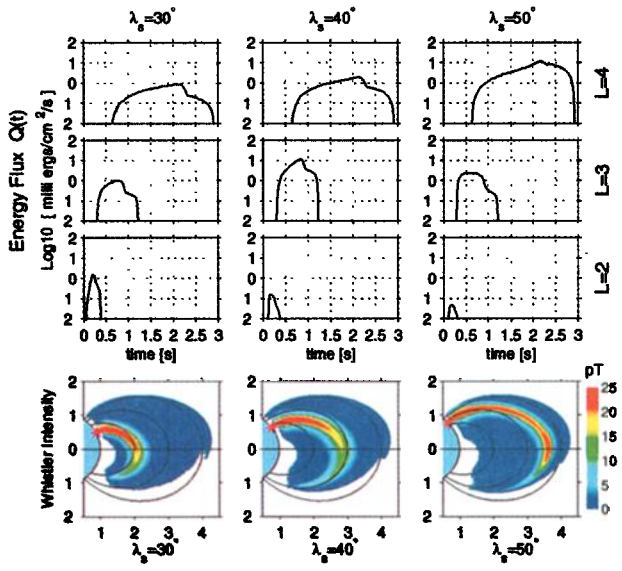

Figure 3. Precipitation energy flux deposited at the foot of L=2, 3 and 4 (upper three panels) for lightning located at magnetic latitudes λ_s=30°, 40° and 50° (left to right) giving rise to the indicated whistler spatial intensity patterns (lower panels, for representative f=5 kHz, shown over all time).

onant particle energies are governed only by the assumed (common) cold plasma properties.

In contrast, the *pulse intensity* variation vs. L-shell directly reflects the lightning source latitude in accord with the whistler spatial intensity pattern. That is, for λ_s=30° the precipitation peak is strongest at L=2 (by a small margin), for λ_s=40° the pulse is strongest at L=3, and for λ_s=50°, at L=4. For λ_s=30° the peak flux at all three L-shells is nearly equal despite the reduced whistler intensities for $L>\sim$2.5 due to the increased physical interaction lengths (which in degrees of λ hold roughly constant) and greater abundance of generally lower resonant energy (and thus more easily deflected) particles at high L-shells. These factors – intrinsic to wave/particle gyroresonance in a dipole magnetic field for such energetic electron spectra – combine to promote generally enhanced scattering efficiencies and greater flux at higher L-shells for equivalent wave intensities at respective L-adjusted resonant frequencies. For λ_s=30° these factors just balance the decreasing wave intensities to maintain nearly constant peak flux over L.

The 1 to 10 milli-ergs/cm^2/s precipitation energy flux levels shown in Fig. 3 are nominally within a factor of only two below those levels for strictly ducted waves [*Chang and Inan*, 1985] having equivalent intensities along each respective L-shell, consistent with the moderate reduction in scattering efficiency which occurs as the wave normal angle becomes non-zero [*Lauben*, 1998]. This result is significant, since it implies that discrete oblique-whistler precipitation should readily produce detectable Trimpi events, at least for the upper range of observed intensities such as presented in Fig. 2.

Considering these precipitation flux vs. time profiles simultaneously incident upon the upper atmosphere over a continuum of L-shells, or equivalently, over a continuum of latitudes (at ionospheric altitudes), the precipitation burst arrives first at low latitudes and moves rapidly poleward with time. To clearly illustrate this effect, a sequence of dynamic precipitation energy flux "hotspots" for energies E>100 keV (these higher energies are understood to be those most effective at producing Trimpi events) are calculated for the three previous lightning sources over field lines $1.6<L<4.2$ for a range of longitudes about the source meridian. Fig. 4 shows the resulting dynamic precipitation hotspots projected over the Eastern United States, where the lightning source magnetic latitudes λ_s=30°, 40° and 50° map to geographic latitudes ~19°, ~29° and ~39° (Rows a, b and c, respectively). The three panels in each row show the instantaneous size and location of the dynamic precipitation hotspot at times just after strong flux onset, during peak flux, and just prior to flux termination.

The tendency of the oblique wave ray paths to cross magnetic field lines from initially lower L-shells to higher L-shells (Fig. 1a) during the first half-hop causes the most intense whistler waves – those originating essentially directly above the lightning discharge – to subsequently arrive near the magnetic equator (where the strongest scattering occurs) at L-shells which are *higher* than that of the source (Fig. 3), thus causing the greatest precipitation flux to occur poleward of the discharge. Specifically, for the lowest latitude source (λ_s=30° or 19° geographic, Row a) the separation between the lightning and the precipitation hotspot center ranges ~15° to ~19°. For the highest latitude source (λ_s=50° or 39° geographic, Row c) this separation diminishes to the range ~6° to ~8°, owing to the tighter field-line convergence at higher L-shells (Fig. 3, lower panels).

More generally, comprehensive calculations for lighting sources distributed over λ_s within and beyond the two values

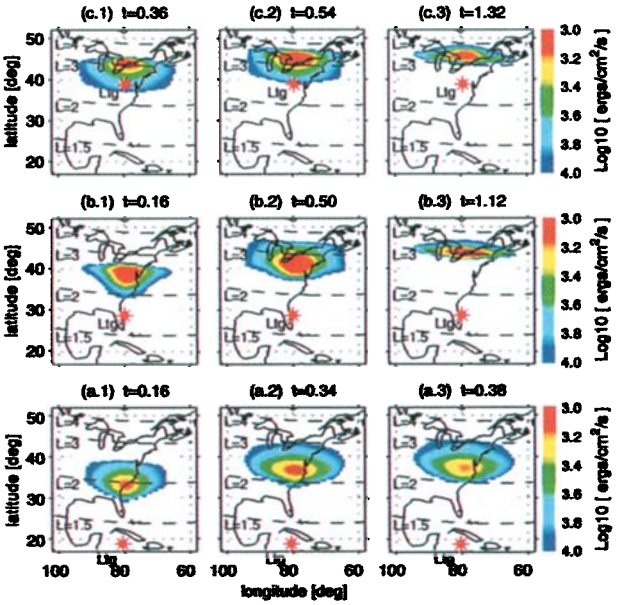

Figure 4. Dynamic precipitation energy flux hotspots (E > 100 keV) for λ_s=30°, 40° and 50° (each row) projected over the Eastern United States. Panels show hotspot size and location at times of strong flux onset, peak and termination (left to right). The distance between the source and hotspot centers diminishes for higher latitude lightning.

presented here show that on average, the net effect of all critical factors of lightning source location, latitude-dependent attenuation, wave/particle resonance conditions, energetic electron distribution, etc., tends to confine the regions of peak (E>100 keV) precipitation to the range $\sim 2 \leq L \leq \sim 3.2$, or equivalently, $\sim 30°$ to $\sim 50°$ geographic latitude (for North American longitudes), remarkably consistent with the observed locations of the vast abundance of Trimpi events detected over the continental United States [*Inan et al.*, 1990].

4. Discussion

The spatial relationships between the source lightning and energetic particle precipitation regions shown in Fig. 4 suggest that several previously reported lightning-induced electron precipitation events may have in fact been produced by oblique whistlers. *Inan et al.* [1990] observed simultaneous perturbations on two subionospheric VLF paths displaced by as much as 3° in latitude having distinctly larger delay observed on the poleward path ($\sim$1.1 s at $L \simeq 2.9$ vs. $\sim$0.65 s at $L \simeq 2.5$) with respect to the causative radio atmospheric. These events were interpreted therein as being due to two separate disturbed ionospheric regions underlying two distinct magnetospheric ducts, the end points of which just happened to be located above the two respective subionospheric paths. In retrospect, it is more likely that these events were produced by a single large oblique-whistler induced-precipitation region such as those shown in Fig. 4, for which the precipitation appears progressively later at higher L-shells with this order of delay (Fig. 3).

In another case, *Yip et al.* [1991] observed a series of VLF perturbation events on a largely east-west path (the disturbed part of the path located at $L \simeq 2.8$) in association with lightning discharges occurring in Midwestern Texas (at $L \simeq 1.8$), while *no* concurrent perturbations were observed on another path passing directly overhead the storm center. This result is entirely consistent with Fig. 4, Row b, in which the precipitation region for such intermediate L-shells is displaced $\geq 10°$ poleward, with peak flux indeed centered over L=2.8.

This result reported by *Yip et al.* [1991] was at the time somewhat puzzling, especially in view of an earlier observation [*Inan et al.*, 1988] of LEP events on a north-south VLF path which directly overlay the active thunderstorm center. In retrospect, noting that the source lightning in that case (*Inan et al.* [1988]) was located at relatively high $L \simeq 2.5$, these two results are actually both consistent with the present calculations in Fig. 4, which show that the precipitation region is indeed closer to the source point for lightning near $L \simeq 2.5$ (Row c) than for $L \simeq 1.8$ (Row b). Thus the events observed by *Inan et al.* [1988] were likely due to disturbed ionospheric regions occurring just slightly poleward of the lightning location while yet lying squarely on the north-south VLF path, thus accounting for the observed strong correlation of LEP event magnitude and occurrence with distance of the source lightning from the disturbed path, as reported therein.

In summary, all three previously published LEP cases appear to be consistent with these new predictions, constituting experimental evidence for the occurrence of widespread poleward-displaced electron precipitation induced by lightning-generated oblique whistlers.

Acknowledgments. This research was supported by the National Aeronautics and Space Administration under grants NAGW-5156 at Stanford, NAS5-30371 via subcontract from the University of Iowa, and by the National Science Foundation under grant ATM-9528173.

References

Chang, H.C. and U.S. Inan, Test particle modeling of wave-induced energetic electron precipitation, *J. Geophys. Res.*, *90*, no. A7, 6409–18, Jul 1985.

Gurnett, D.A., Persoon A.M. Randall R.F. Odem D.L. Remington S.L. Averkamp T.F. Debower M.M. Hospodarsky G.B. Huff R.L. Kirchner D.L. Mitchell M.A. Pham B.T. Phillips J.R. Schintler W.J. Sheyko P. and D.R. Tomash, The POLAR Plasma Wave Instrument, *Space Science Reviews*, *71*, no. 1-4, 597–622, Feb 1995.

Helliwell, R.A., *Whistlers and Related Ionospheric Phenomena*, Stanford Univ. Press, Stanford, CA, 1965.

Inan, U.S. and T.F. Bell, The plasmapause as a VLF wave guide, *J. Geophys. Res.*, *82*, no. 19, 2819–27, Jul 1977.

Inan, U.S. and D.L. Carpenter, On the correlation of whistlers and associated subionospheric VLF/LF perturbations, *J. Geophys. Res.*, *91*, no. A3, 3106–16, Mar 1986.

Inan, U.S., Shafer D.C. Yip W.Y. and R.E. Orville, Subionospheric VLF signatures of nighttime D region perturbations in the vicinity of lightning discharges, *J. Geophys. Res.*, *93*, no. A10, 11455–72, Oct 1988.

Inan, U.S., Knifsend F.A. and J. Oh, Subionospheric VLF 'imaging' of lightning-induced electron precipitation from the magnetosphere, *J. Geophys. Res.*, *95*, no. A10, 17217–31, Oct 1990.

Lauben, D. S., *Precipitation of Radiation Belt Electrons by Obliquely-Propagating Lightning-Generated Whistler Waves*, Ph.D. Dissertation, Stanford University, Stanford, CA, 1998.

Poulsen, W.L., Inan U.S. and T.F. Bell, A multiple-mode three-dimensional model of VLF propagation in the Earth-ionosphere waveguide in the presence of localized D region disturbances, *J. Geophys. Res.*, *98*, no. A2, 1705-17, Feb 1993.

Rastani, K., Inan U.S. and R.A. Helliwell, DE 1 observations of Siple transmitter signals and associated sidebands, *J. Geophys. Res.*, *90*, no. A5, 4128–40, May 1985.

Ristic-Djurovic, J.L., Bell T.F. and U.S. Inan, Precipitation of radiation belt electrons by magnetospherically reflected whistlers, *J. Geophys. Res.*, *103*, no. A5, 9249–60, May 1998.

Yip, W.-Y., Inan U.S. and R.E. Orville, On the spatial relationship between lightning discharges and propagation paths of perturbed subionospheric VLF/LF signals, *J. Geophys. Res.*, *96*, no. A1, 249–58, Jan 1991.

D. S. Lauben, U. S. Inan and T. F. Bell, STARLab, Stanford Univ., Stanford, CA 94305-9515. (email: dsl@polar.stanford.edu)

(Received January 30, 1999; accepted March 15, 1999.)